



VLF lightning location by time of group arrival (TOGA) at multiple sites

Richard L. Dowden *, James B. Brundell, Craig J. Rodger

LF-EM Research Ltd., 161 Pine Hill Road, Dunedin, New Zealand

Received 6 June 2001; received in revised form 23 January 2002; accepted 15 March 2002

Abstract

Lightning is located by using the time of group arrival (TOGA) of the VLF (3–30 kHz) radiation from a lightning stroke. The dispersed waveform (“sferic”) of the lightning impulse is processed at each receiving site. The TOGA is determined relative to GPS at each site from the progression of phase versus frequency using the whole wave train. Unlike current VLF methods which require transmission of the whole wave train from each site to a central processing site, the TOGA method requires transmission of a single number (the TOGA) for lightning location calculation. The stable propagation and low attenuation of VLF waves in the Earth–ionosphere waveguide (EIWG) allows a wide spacing of receiver sites of several thousand kilometer so that a truly global location service could be provided using only ~10 receiver sites. © 2002 Elsevier Science Ltd. All rights reserved.

Keywords: Lightning location; Time of arrival; Time of group arrival; Arrival time difference; Earth–ionosphere waveguide; Omega navigation

1. Background

Lightning location systems using networks of radio receivers are of two main classes. The first class uses magnetic direction finding from each receiving station and the second class uses the difference in the times of arrival of the lightning radio impulse (“sferic”) at each independent pair of receiving stations. In this paper we are concerned only with the second class.

1.1. Systems using timing only

The so-called time of arrival (TOA) system (Lewis et al., 1960), the modern form of which is lightning position and tracking system (LPATS) (Casper and Bent, 1992), uses the TOA of the leading edge of the lightning pulse at each station. Since only the first few microseconds of the lightning

pulse or wave train are used to avoid the sky wave (that reflected off the ionosphere) which arrives slightly later, the essential information is in the MF band (0.3–3 MHz) even if the bandwidth of the receivers extends down to 1 kHz. Since the lightning pulse is dominated by the return stroke (ground to cloud), this allows location of the ground point of the lightning strike to within a few hundred metres (Cummins et al., 1998; Cummins and Murphy, 2000). Such accurate location is important for insurance inspectors checking claims and for power line companies locating line faults. It requires a tight network of ground stations with separations of a few hundred kilometer since this technique relies on ground wave propagation which has high attenuation at the high frequencies used. Thus the US national lightning detection network (NLDN) (Cummins et al., 1998) uses ~100 ground stations to cover the contiguous US (~10⁷ km²), corresponding to a ground station density of ~10 Mm⁻². This high density of ground stations is not commercially feasible for large areas of low population density or over oceans.

A subclass of this type uses the VLF band (3–30 kHz) which contains the highest power spectral density of lightning radiation (Malan, 1963; Pierce, 1977). Lightning is

* Corresponding author. Tel.: +64-3-473-0521; fax: +64-3-473-0526.

E-mail address: dowden@physics.otago.ac.nz (R.L. Dowden).

easily detected and measured at VLF at ranges of several thousand km. Propagation over such ranges in the EIWG disperses the initial sharp pulse of the lightning stroke into a wave train lasting a millisecond or more. The amplitude of the received wave train (“sferic”) rises slowly (a few hundred microseconds) from the noise floor, so there is no sharp onset and no sharply defined TOA. To get adequate accuracy of a meaningful time of arrival, or rather the difference in the times of arrival of the sferic at each pair of receiver sites, the whole VLF wave train is used.

There are two ways of using the whole VLF wave train for timing measurement. The one in commercial use measures the arrival time difference (ATD) by cross-correlation of the full VLF wave trains received at a pair of sites (Lee, 1986a, b, 1989). The second way, which is the subject of this paper, measures the rate of change of the sferic phase with respect to frequency at the trigger time to find the time of group arrival (TOGA) at each receiver site.

1.2. Lightning location by timing alone

For all methods of radio location using only timing, and thus not including direction finding, three independent pairs of sites, and so at least four sites, are needed for unambiguous location. Only the difference in arrival times at each pair of sites of a sferic from a common lightning strike is of relevance since the absolute time of the lightning strike can be deduced from these difference in arrival times only after the lightning strike has been located. This is the case when an individual time of arrival (TOA or TOGA) can be determined for each sferic, so the difference is simply the difference between the two times, as well as when the sferic waveforms from a pair of sites are processed together to determine the ATD for that pair without seeking individual arrival times.

Although there is no sharply defined TOA at VLF, the sferic can be detected when the amplitude of the wide band signal rises above the background. We have found it more effective to use the rate of change of the amplitude as the detection criterion. The wide band signal is sampled at about 50 kHz, so consecutive samples are about 20 μ s apart. We monitor the magnitude of the difference between consecutive samples, i and $i + 1$, and when this exceeds a set threshold value, the time of the second sample (that of $i + 1$) is recorded as the “trigger time”, t_0 . As discussed later, this time can be measure relative to the pulse-per-second (PPS) of the Global Positioning System (GPS) to within a few hundred nanoseconds. The trigger time, t_0 , is not the TOGA but is within 100 μ s of the TOGA which is near enough for the following example of lightning location at VLF by timing alone.

Currently our TOGA network consists of only six VLF receivers. These are located at Dunedin (45.9°S, 170.5°E), Perth (32.1°S, 115.8°E), Darwin (12.4°S, 130.9°E), Brisbane (27.6°S, 153.1°E), Osaka (34.8°N, 135.5°E), and Singapore (1.3°N, 103.8°E). These sites (except for Osaka and Singapore which are off the map) are shown as asterisks in Fig. 1.

In this example, the lightning strokes were located from the trigger times at each of these sites using the downhill simplex method (Nelder and Mead, 1965) of successive approximations. The starting point is that of the site of the VLF receiver which received the sferic first (the earliest trigger time). For this and all later points in the iterative process, the group travel time from the point to each of the VLF receiver sites is calculated and compared with the observed time of arrival (in this example, the trigger time). This gives the errors and the “downhill” direction for locations reducing the errors. Although this process typically requires about 100 iterations, current PCs can do this in a few milliseconds. This process gives both the lightning stroke position and the likely error.

Fig. 1 shows the positions of 46 lightning strokes as open circles. All strokes occurred during the 10-min period from 01:50 to 02:00 UT. This is early afternoon at 180°E longitude (right-hand limit of the map) and mid-morning at 105° longitude (left-hand extreme), so all paths are in daylight. Position errors due to using of the trigger time instead of the TOGA are much less than the resolution of the map as printed.

Despite popular belief, lightning often does strike in the same place. Note the thick circle in Fig. 1 about 500 km south west of Darwin, just over the Western Australian border. The thickness is due to several strokes almost superimposed. Lee (1989) found that intense thunderstorms produce such clusters of lightning strokes and used them to test his method of VLF lightning location. On another occasion (not shown here), we found a cluster of 52 strokes centred on 11.9°S, 62.7°E, comprising 13% of all strokes recorded on the six-station network over the 20-min period. This shows that lightning can be located by VLF at ranges of 10 Mm from the further VLF receivers (Dunedin and Osaka) of our network, even when all paths are in daylight.

2. TOGA determined by phase slope

2.1. Need for TOGA

The trigger time, t_0 , is an adequate substitute for the TOGA in some studies, but introduces both random and systematic errors. Random errors of up to 20 μ s arise because the trigger time is digitised in approximately 20 μ s steps, the reciprocal of the sampling frequency (some sound cards sample at 48 kHz, some at 50 kHz). Systematic errors arise because the trigger threshold is reached earlier in the waveform of a strong sferic than in that of a weak sferic. A sferic from a given lightning stroke is strongest at the nearest receiver and weakest at the furthest receiver, producing an early trigger at the closest and a late trigger at the furthest.

The trigger time, t_0 , is precisely defined as a certain point in the digitised VLF sferic waveform. It can be determined, as we will see, to within a few hundred nanoseconds. Our task is therefore to seek a correction (positive or negative) to add to t_0 to get the TOGA.

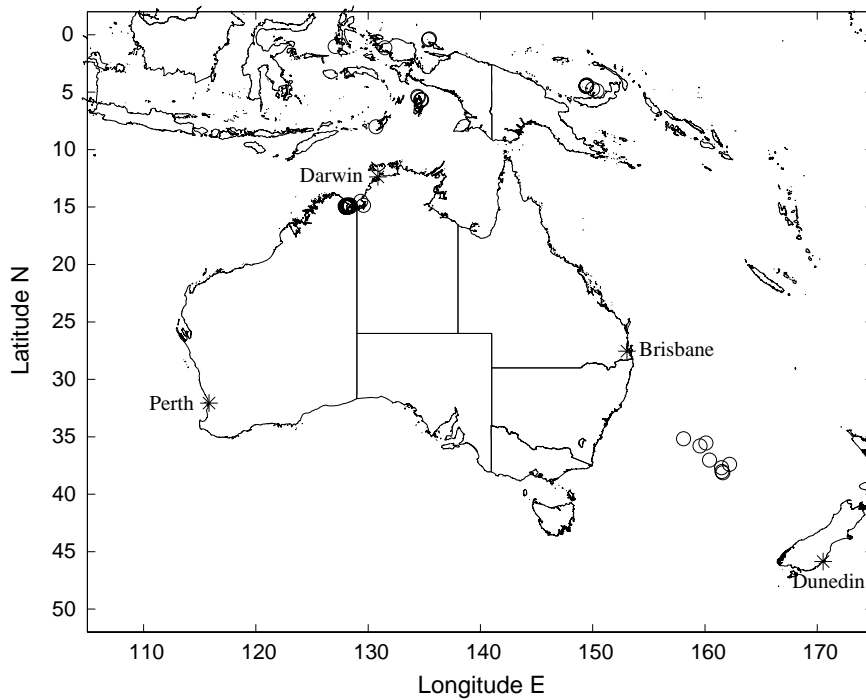


Fig. 1. Lightning location using the six VLF receiver sites currently available. Four of these are indicated on the map by an asterisk (*). The Singapore site is just off the map near the top left corner, while Osaka (Japan) is well to the north. The locations of the 46 strokes during 01:50–02:00 UTC (about local midday) on 22 December, 2001, are shown by open circles, many of which are almost coincident on this scale and appear as thickened circles.

2.2. Basic theory

The current in a typical lightning return stroke reaches its peak value in about 2 μ s and decays to half peak in about 40 μ s (Uman, 1983). This results in a short pulse of ~ 100 μ s covering a very wide band from ULF to optical frequencies. Lee (1989) points out that effectively all the VLF power from the first return stroke comes from the lowest 2 km, which is a small fraction of a wavelength in the VLF band (10–100 km), so the source of the VLF radiation is a short current element. Thus, we can assume that the phase of all the VLF Fourier components of the current is the same so that the initial (at zero range) phase is the same (ϕ_0) for all the VLF Fourier components of the radiated electric field. Since the vertical component of the stroke current dominates as far as VLF propagation in the EIWG is concerned (Lee, 1989), and the current is often nearly vertical anyhow for the lowest few hundred metres (Krider et al., 1976), we would expect ϕ_0 in Eq. (2) below to be zero or π , but the value of ϕ_0 is of no consequence as we will see in Eq. (3). At range r from the lightning stroke and at time t , the wave field can be expressed as

$$E(r, t, \omega) = \sum A(\omega) \cos(\phi(\omega)), \quad (1)$$

where, at any one Fourier component of frequency ω ,

$$\phi(\omega) = \omega t - k(\omega)r + \phi_0 \quad (2)$$

and the wave vector, k , is dependent on frequency while the phase, ϕ_0 , is not. Differentiating with respect to frequency at any time, t , and range, r , we find,

$$\frac{d\phi}{d\omega} = t - r \frac{dk}{d\omega} = t - \frac{r}{v_g(\omega)}, \quad (3)$$

where $v_g(\omega)$ is the frequency-dependent group velocity.

From the definition of group velocity, the time, $t_g(\omega)$, taken by the wave group to travel from the lightning source (the return stroke) to the receiver at range r is $r/v_g(\omega)$. This group travel time is frequency dependent though not strongly so if we restrict measurement to frequencies well above the EIWG cutoff of the dominant waveguide mode. From Eq. (3), $d\phi/d\omega$ is zero when $t = t_g(\omega)$. This means that the group travel time at frequency ω , namely $t_g(\omega)$, might be found on this criterion by trial and error. However, it is simpler to measure $d\phi/d\omega$ at a single known time, t_0 . Then

$$t_g(\omega) = t_0 - \frac{d\phi}{d\omega}. \quad (4)$$

As will be explained in Section 3.3, t_0 is a precisely known absolute time (UT) determined from the GPS pulse-per-second (PPS). This is known to be ± 100 ns

(Trimble, 1999) now that the SA (selective availability) has been removed by the US Department of Defense which operates and maintains the GPS.

If the spectral energy of sferics was always concentrated in a narrow band centred on frequency, ω_a , we could use Eq. (4) to determine the TOGA from the phase slope, $d\phi/d\omega$, at ω_a and at time t_0 . As we will see later in Section 4.1, the average smoothed spectrum of sferics as observed on our receivers shows a maximum at about 10 kHz with a 3 dB bandwidth of 14 kHz. While this suggests that the TOGA should be defined as $t_g(10 \text{ kHz})$, estimation of the phase slope at a single frequency requires phase measurement over a finite range of frequency (this applies to real data but not to the mathematical model presented later in Section 2.3). For maximum utility of the data we fit a least-squares regression line to the $\phi(\omega)$ data set spanning the frequency range from 6–22 kHz. The slope of this regression line is our best estimate of $d\phi/d\omega$ for substitution in Eq. (4) to calculate the TOGA. If instead of measuring $\phi(\omega)$ at t_0 , we measured it at the TOGA, Eq. (3) requires that the regression line has zero slope. We therefore define the TOGA as:

The TOGA of a sferic is that instant when the regression line of phase versus frequency over a specified band has zero slope. This instant depends on the frequency band specified. We choose the band 6–22 kHz because it is the band of highest sferic amplitude. For lightning location purposes, the choice of band is not very important provided the band is the same for all sferics.

Note that the TOGA is an absolute time in UTC (or other standard) whereas $t_g(\omega)$ is the time taken (at frequency ω) to travel from the lightning stroke to the VLF receiver. If the lightning stroke occurs at absolute time, t_s , in UTC, the relationship is,

$$\text{TOGA} = t_s + \overline{t_g(\omega)}, \quad (5)$$

where the bar implies an average over the band 6–22 kHz. Eq. (5) is of no use as a definition of the TOGA since neither of the times on the right-hand side is known initially, and can only be calculated after the lightning stroke is determined. To avoid any confusion we will use the term TOGA as in Eq. (5) instead of defining a symbol for the time of group arrival.

2.3. Synthetic sferics

Consider a simple form (parallel plate) of TM waveguide propagation dispersion determined by the dispersion equation (Cheng, 1983),

$$k^2 = (\omega^2 - \omega_0^2)/c^2, \quad (6)$$

where ω_0 is the cutoff frequency, which for a typical night-time ionosphere is about 1.67 kHz for the first-order mode. This gives the phase velocity,

$$v_p = \frac{\omega}{k} = \frac{c}{\sqrt{1 - \omega_0^2/\omega^2}}. \quad (7)$$

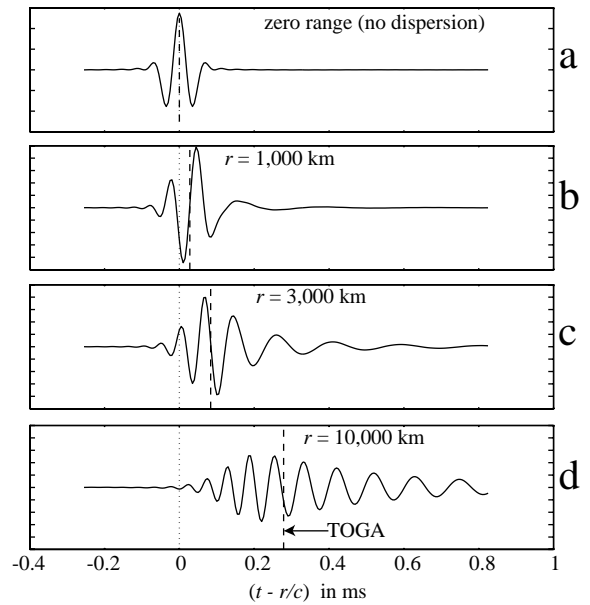


Fig. 2. Model pulse according to Eqs. (8) and (9) produced by adding 100 waves over the range 2–24 kHz. This limited frequency range and the weighting function (Eq. (9)) models the typical lightning spectrum and our amplifier and sound card response. The phase velocity of the component waves is frequency dependent according to the TM mode but always $>c$. The wave packet travels at $<c$ and expands with distance, r . The vertical dashed line in each of the panels indicates the TOGA relative to the speed-of-light arrival time, $t = r/c$.

We now consider a sum of 100 cosines, each having the form

$$A(\omega)\cos\left[\omega\left(t - \frac{r}{v_p}\right)\right] \\ = A(\omega)\cos\left\{\omega\left[t - \frac{r}{c}\sqrt{1 - \omega_0^2/\omega^2}\right]\right\}, \quad (8)$$

where $A(\omega)$ is a weighting function which approximates the power spectrum of lightning sferics,

$$A(\omega) = \cos^2\left(\pi\frac{\omega - \omega_a}{2\omega_r}\right), \quad (9)$$

where ω_a is the frequency of peak spectral density and ω_r is chosen to correspond to the bandwidth of 14 kHz so that the half power frequencies, 5 and 19 kHz, are reasonably typical of sferic spectra.

The weighted sum of these 100 is shown in Fig. 2 for various ranges, r . In Fig. 2(a), $r = 0$, so the form of the pulse is symmetrical since there is no dispersion. This gives rise to the negative swings on either side of the central maximum. It should be noted that $t = 0$ is defined by $d\phi/d\omega = 0$ where all 100 frequency components are in the same phase ($\phi_0 = 0$ in this case).

In Figs. 2(b), (c), and (d), $r = 1, 3$ and 10 Mm, respectively. The time scale in all panels of Fig. 2 is the same with

a vertical line of dots to indicate $t - r/c = 0$, or where the centre of the original pulse would be if it had not been dispersed. Note that the concept of a sharp TOA is of little use at VLF because the spheric amplitude grows relatively slowly from an ill defined background to a maximum. This is particularly noticeable in Fig. 2(d) where this growth is over a period of 200 μ s. The “time of group arrival” (TOGA), as defined at the end of Section 2.2, is marked in Fig. 2 by the vertical dashed line.

Only for non-dispersive propagation (as in the TEM mode) does the pulse propagate without change in shape, so at all times and ranges, $d\phi/d\omega$ is then independent of frequency and is zero at $r = ct$ where all frequency components are in the same phase. For dispersive propagation of any kind, the phase velocity is frequency dependent so the wave number, k , is not proportional to frequency, ω . Consequently, $dk/d\omega$ must be frequency dependent and, from Eq. (3), so must $d\phi/d\omega$. A pulse synthesised by a wide spectrum such that all components are in phase at $t = 0$, $r = 0$, and propagating in a dispersive medium, can never again have all its components in phase.

For any of the parallel plate waveguide modes, apart from the non-dispersive TEM mode, we get from Eqs. (3) and (7)

$$\frac{d\phi}{d\omega} = t - \frac{r}{c} \sqrt{1 - \frac{\omega_0^2}{\omega^2}} \quad (10)$$

If we take the speed-of-light time, $t = r/c$, we get

$$\left. \frac{d\phi}{d\omega} \right|_c = \frac{r}{c} \left(1 - \sqrt{1 - \frac{\omega_0^2}{\omega^2}} \right) \quad (11)$$

It is more useful to plot $\phi(\omega)$ rather than the derivative given by Eq. (11). From the right-hand side of Eq. (8), and again for the speed-of-light arrival time, $t = r/c$, we get

$$\phi|_c = \omega \frac{r}{c} \left(1 - \sqrt{1 - \frac{\omega_0^2}{\omega^2}} \right) \quad (12)$$

Fig. 3(a) shows $\phi(\omega)$ for $r = 1000$ km. The plot of $\phi(\omega)$ for any other range looks exactly the same as this except for the scale of ϕ . Thus for $r = 10$ Mm, the only difference is that the numbers on the ϕ scale are exactly 10 times larger. This is because both the phase (Eq. (12)) and its derivative (Eq. (11)) are directly proportional to the range, r . In practice (for analysis of sferics), we consider only frequencies well above any of the waveguide cutoff frequencies so we do the same in this synthesis. In practice the highest frequency must be less than half the sampling frequency (usually 48 kHz), so to be consistent with this we plot $\phi(\omega)$ only over the frequency range 6–22 kHz in Fig. 3(a). Dividing both sides of Eq. (12) by 2π changes the phase and frequency from radian units to the more familiar cycle units as presented in Fig. 3.

The regression line or least-squares linear fit in Fig. 3(a) (long dashed line) has the same slope as the $\phi(\omega)$ curve at

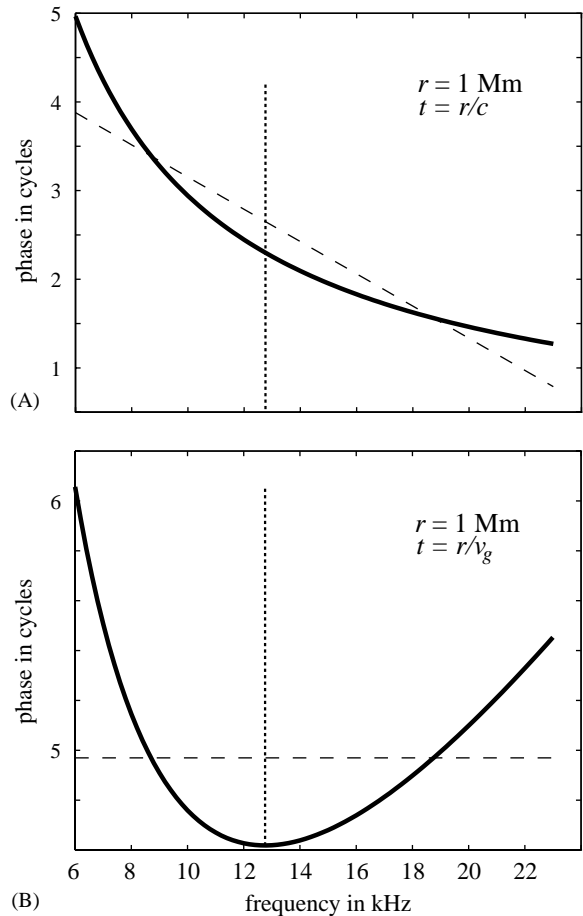


Fig. 3. Upper panel (a) shows the phase versus frequency (solid curve) at time $t = r/c$ of the synthetic spheric shown in Fig. 2(b). The corresponding curves for the other synthetic sferics (c and d) are identical to this one. Only the phase scale is changed. The long dashed line is the least squares regression line, the slope of which defines the TOGA indicated in Fig. 2(b). Lower panel (b) shows the phase versus frequency at time $t = r/v_g$, where v_g is the group velocity at 12.757 kHz. This frequency (indicated by the vertical dotted line in both panels) was chosen for the band averaged value of $v_g = 0.9914c$ to make $t = r/v_g =$ the TOGA as indicated by the zero slope of the least-squares regression line.

~ 13 kHz (actually at 12.757 kHz as indicated by the dotted line). This is the case for all ranges since the shape of the $\phi(\omega)$ curve is range independent. In this theoretical model, the phase slope can be calculated at a single frequency by Eq. (11). Since the calculated slope at 13 kHz matches that of the regression line quite well, we use phase slopes calculated at 13 kHz to determine the positions of the TOGA on the time scales in Fig. 2 where they are marked by dashed vertical lines.

It is important to note that the phase slope depends on the instant, t , at which it is measured, as is clear from Eq. (10). Fig. 3(a) is calculated for $t = r/c$. Fig. 3(b), on the

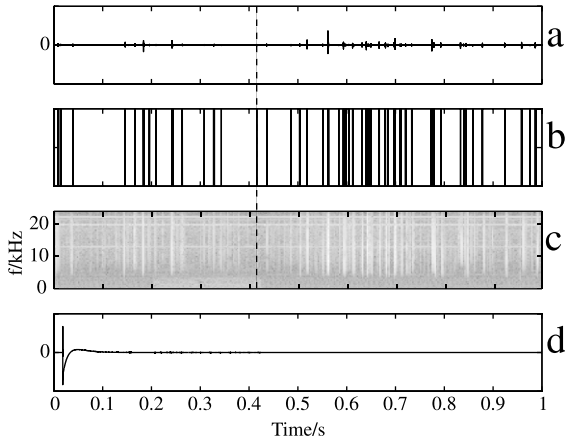


Fig. 4. A single second of the sound card output at Darwin, Australia. (a) and (c) show the broad band (2–24 kHz) VLF output as electric field (arbitrary linear units) and as spectrogram, respectively. The sferics are seen in (c) as vertical lines rarely extending below 5 kHz and in (a) as bipolar spikes. The vertical lines in (b) mark the times of detected sferics. (d) shows the GPS pulse-per-second (PPS) band limited to 24 kHz by the sound card.

other hand, is calculated for the TOGA or, in this model, for $t = t_g(12.757 \text{ kHz})$, while r remains the same (1 Mm). The frequency 12.757 kHz was found by requiring that the right-hand side of Eq. (10) be zero so that the regression line be precisely horizontal as shown. This occurs at the slightly later group-speed time, $t \sim 1.008r/c$.

3. The TOGA method

3.1. VLF receiver configuration

All our current and planned TOGA sites are in built-up areas unsuitable for use of magnetic loop antennas at VLF because power line harmonics would dominate the sferic magnetic field. However, at VLF even poor conductors such as ferroconcrete buildings remain at ground potential and shield man-made electric fields generated within them. Consequently we use a short (1.5 m) whip antenna on a tall building at each site to measure the vertical electric field of the TM modes present. Since the sferic wavelength near the upper frequency is 15 km, such a whip antenna is purely capacitive ($\sim 15 \text{ pF}$) and so wide band. A nearby GPS antenna and receiver provide the PPS signal and a time code for maintaining the computer's clock to within about 10 ms. The amplified VLF signal and GPS PPS signal are fed to a stereo sound card in the computer. Fig. 4 shows a single second of the sound card output at Darwin, Australia. The strong 19.8 kHz signal from the VLF transmitter (call sign, NWC) which is 2000 km distant, has been filtered down by about 20 dB. Figs. 4(a) and (c) show the broad band (2–24 kHz) VLF output by sample value (electric field) and by

spectrogram, respectively. The upper limit is determined by the sampling frequency of about 48,000/s. The sferics are seen in Fig. 4(c) as vertical lines, usually ending at about 5 kHz. Several VLF transmission signals are seen in Fig. 4(c) as horizontal lines or segments. However, by reducing the NWC signal, the total contribution of such signals to the broad band background is insignificant as can be gauged by the thinness of the horizontal line in Fig. 4(a). The bipolar spikes in Fig. 4(a) are sferics and so correspond to those in the spectrogram.

3.2. Sferic detection

The 48,002 first differences of the 48,003 samples of VLF electric field, $E(i)$, in this particular second in Fig. 4, can be expressed as $\Delta E(i)$ where i is the sample index or number, 1–48,002. Thus

$$\Delta E(i) = E(i) - E(i - 1) \quad (13)$$

is defined so that the index refers to the second sample of a pair. We take the modulus of these differences, $|\Delta E(i)|$, and determine the mean of the 48,002 moduli. Then all moduli, $|\Delta E(i)|$, greater than N times the mean, trigger the capture of a sferic of 64 samples (1.3 ms) provided the trigger time is at least 2 ms after the previous trigger to avoid overlapping. The value of N is set manually or automatically for optimum detection efficiency, so it varies geographically from site to site and temporally both diurnally and seasonally. Trigger times for $N = 10$ are shown as the vertical lines in Fig. 4(b). These times are according to the computer clock which was “fast” by about 16 ms at this time. Provided the computer clock is within 500 ms of UT to avoid an error of a full second, we need only the trigger sample index, I_{tg} , for determination of the trigger time, t_0 , to within $1 \mu\text{s}$ as we will see in Section 3.3 below.

3.3. Trigger time (t_0)

We have found that our sound card sampling frequency is quite stable over a few minutes so the sampling acts as a clock. We will regard the “ticks” of this clock as the sampling instants. We also need its phase (the “time” of the clock: by how much it is “fast” or “slow”). As we will show later in this section, this phase can be measured every second by GPS to within $0.1 \mu\text{s}$ of UT. During the exact second between successive GPS pulses, we not only count the integer number of ticks (samples) but also measure the sampling phase at the start and end of this interval of $1,000,000.0 \pm 0.1 \mu\text{s}$. Thus in a single second we measure the sampling frequency to within about 1 part in 10^7 and determine the instant of each and every tick or sampling instant to well within $1 \mu\text{s}$ of UT.

The output voltage of the VLF receiver at each site is sampled continuously by the sound card. The voltage difference between successive samples is continuously monitored. If the absolute voltage difference exceeds a set

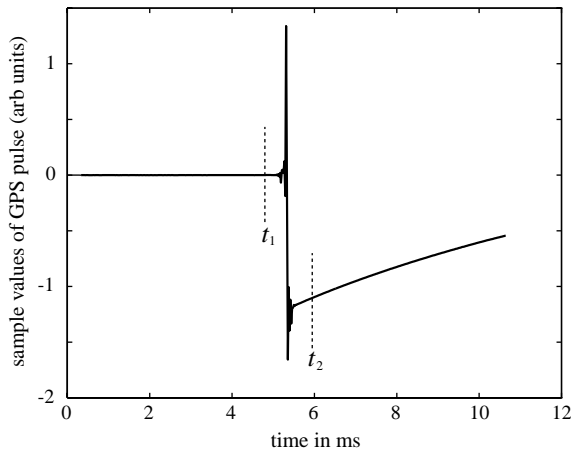


Fig. 5. 512 samples (~ 10.7 ms) centred on the spike of the GPS PPS shown in Fig. 4(d). The vertical dotted lines mark arbitrary times, t_1 and t_2 , earlier and later than the GPS PPS, respectively, for discussion in the text.

threshold, sferic capture is triggered and the instant of taking the sample causing this triggering is called the “trigger time”, t_0 . Like every sample instant, t_0 is known to well within $1 \mu\text{s}$ of UT as shown in the previous paragraph. The name or index of this sample is I_{tg} .

We now see how to find the sampling phase (the time of the clock). At the sample frequency of about 48,000/s, the samples are some $20 \mu\text{s}$ apart, so it might seem that the GPS PPS pulse of only $10 \mu\text{s}$ duration could easily slip between two samples $20 \mu\text{s}$ apart. However, Fig. 4(d) shows the GPS PPS band limited to 24 kHz by the sound card, so that with the accompanying ringing its duration is nearly 100 ms or some 4000 samples. Fig. 5 shows a section (10.66 ms long) of Fig. 4(d) with higher time resolution. This section consists of 512 samples centred on the maximum value in the PPS channel. The index (indicated by #) of this maximum value in the whole 48,003 samples (the whole second) turned out to be #758.

The instant of sample #758 can be calculated in terms of the sampling clock. However, this determines the time of the GPS PPS in terms of this clock only to within $\pm 20 \mu\text{s}$. To find it to within $\pm 0.1 \mu\text{s}$, we use the same phase slope ($d\phi/d\omega$) technique that we used in Section 2.2 to find the TOGA. In this case there is almost no dispersion or phase distortion and no noise.

We take the discrete Fourier transform (DFT) of this section of 512 samples. This gives the phase and amplitude of the 256 component cosines which all have almost the same phase at some point in time which we need to find out as it is the GPS zero (the PPS instant). Since the DFT is an integral over time (10.66 ms in this case), the amplitude spectrum applies to the whole time and tells us nothing about how the spectrum might have varied during this time. But what about the phase spectrum? We know by definition that

all 256 component cosines have the same phase at the PPS instant (we will call this zero for the present discussion). At all *later* times, such as at t_2 in Fig. 5, the phase at all frequencies will have *increased* by ωt_2 , so the slope, $d\phi/d\omega$, must be *positive*. At all *earlier* times, such as at t_1 in Fig. 5, the phase at all frequencies will have *decreased* by ωt_1 , so the slope, $d\phi/d\omega$, must be *negative*. As a check on this interpretation, we note that the phase slope in Fig. 3a is negative at the speed-of-light time which must be earlier than the TOGA (in Fig. 3b) when this slope (or rather that of the regression line) is zero.

Like the amplitude spectrum, the phase spectrum does not contain the time explicitly, yet we know that the phase spectrum must vary continuously throughout the interval (10.66 ms in this case) of the integration. The answer to this paradox is that the DFT “knows” that all phases increase with time as ωt so it presents the phase spectrum extrapolated back to the time of the first sample of the 512. To find the phase spectrum at any other time, such as t_1 in Fig. 5, we add the constant time, t_1 , to the time in the integral. This is simply achieved by term-by-term vector multiplication of the DFT series in ω by the series in ω of $\exp(i\omega t_1)$.

In principle we can choose any time at which to get the phase spectrum, but for best accuracy it should be that of the sample nearest the time of the PPS instant. This is likely to be that of the sample of maximum value, which is #758 of the set of 48,003 and so #256 of the selected 512.

Using this time in the DFT, we get the phase versus frequency plot shown in Fig. 6. To remove end effects, we use a cosine squared window and restrict the frequency range to 6–22 kHz. From the slope ($d\phi/d\omega$), which is *positive*, the PPS occurred $8.4 \pm 0.1 \mu\text{s}$ *before* sample #758 (thus like t_2 in Fig. 5, the instant of sample #758 was *after* the PPS instant). The calculated error (actually $0.08 \mu\text{s}$) assumes that the small wave-like departure from the regression line is random noise. Actually, this trivial error is a fixed offset, not a random error, and is calibrated out as discussed later in this Section 3.3.

Since many sferics occur in a single second, it makes sense to establish one time scale for each second for all the sferics in it. So having established that the instant of sample #758 was at $8.4 \mu\text{s}$, we can deduce that the instant of virtual sample #0 was $-15,782 \mu\text{s}$, knowing that the sampling frequency at the time of the second in Fig. 4 was 48,003.143/s, or one sample every $20.832 \mu\text{s}$. Thus, for the sferic marked in Fig. 4 by the vertical dashed line, which was detected at about 0.42 s according to the computer clock, and was “triggered” at sample $I_{\text{tg}} = \#19,959$, we find $t_0 = 415,786 \mu\text{s}$.

Only the leading edge of the GPS PPS is “true”. The trailing edge is $10 \mu\text{s}$ later. The time determined by $d\phi/d\omega = 0$ refers to the middle of the PPS pulse so is $5 \mu\text{s}$ late. In addition, there is the delay of the VLF signal (the sferic) through the VLF preamplifier and electronics not shared by the PPS signal. While these delays or offsets would not be serious if they were the same at every site, we effectively remove all such time offsets, and in addition obtain both the amplitude

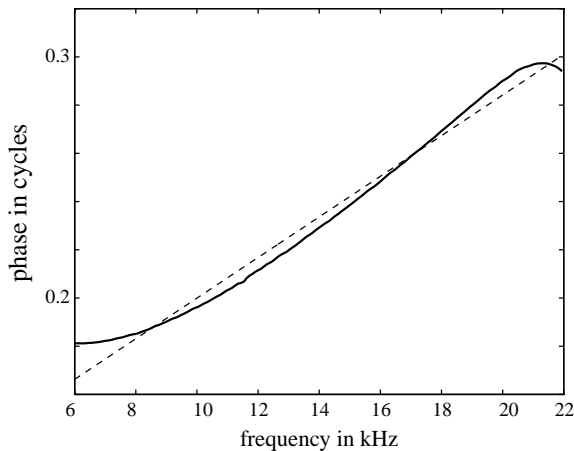


Fig. 6. Phase versus frequency (solid curve) at the instant of the sample having the maximum value (spike top) of the GPS PPS. The slope of the regression line (dashed) is used to find the exact time of this sample instant relative to the GPS PPS. This, together with a precise determination of the sampling frequency, establishes a precision time base for this particular second. The curved departure from the regression line is due to the phase response of the sound card, particularly at the highest (half the sampling frequency) and lowest frequencies. The frequency range is restricted to 6–22 kHz to minimise these effects which produce an error in slope determination of only 80 ns.

and phase response of the full VLF receiving system, including the sound card, by the use of an additional custom-built, hand-held GPS receiver to inject a GPS synchronised signal (sharp rise followed by exponential decay) directly into the VLF antenna or the equivalent dummy antenna (a 15 pF capacitor). From there the “artificial sferic” traverses the same path through the system as does each real sferic and so must suffer the same delays. Using exactly the same method of analysis as used for determining the TOGA of a real sferic, the TOGA of this artificial sferic is found to be 20 μ s for all stations using the standard receiving equipment. As a check, the phase response was found using monochromatic signals (sine waves) as shown in Fig. 7. Only the frequency range, 6–23 kHz, is used to determine the regression line, the slope of which determines the delay to be 20 μ s. As a further check, this delay was measured to be \sim 20 μ s using a two-channel oscilloscope.

3.4. Phase slope measurement

Fig. 8(a) shows the phase versus frequency ($\phi(\omega)$) of a sferic captured in Darwin, Australia determined at the instant of capture (t_0). The phase plot is limited to the frequency range of 6–22 kHz for two reasons. Firstly, we want the lowest frequency to be well above the EIWG cutoff frequency to reduce the effect of EIWG dispersion. Secondly, the highest frequency must be less than half the sampling frequency (24 kHz) to avoid Nyquist folding, and apprecia-

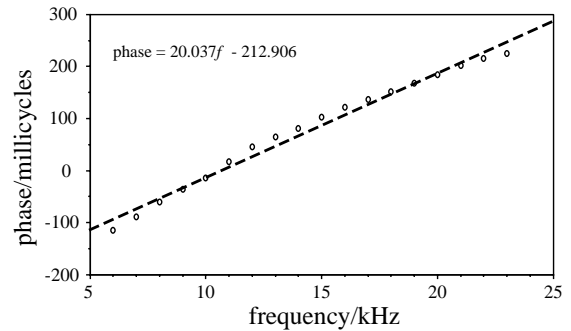


Fig. 7. Phase response of the TOGA receiver from the VLF antenna to the computer sound card input. This is the total path not common to the GPS pulse-per-second (PPS). This response was measured at the discrete frequencies, 6–23 kHz in 1-kHz steps, as indicated by the 0-shaped points. The regression line slope shows that the receiver path delay is 20.037 μ s, in agreement with GPS pulse measurements.

bly less to avoid the large $d\phi/d\omega$ near this frequency. A less important reason is that this frequency range includes most of the spectral energy of sferics as we will see in Section 4.1.

The phase is measured at t_0 , the sferic capture or trigger time which in this case occurred just before the measured TOGA. Over the frequency range chosen, the phase varies only 0.7 cycles (\sim 250°) but falls steeply with frequency at the low frequency end and rises at the high frequency end. This behaviour is similar to that shown in Fig. 3(a) for the synthetic sferic, but the average slope (indicated by the regression line) is much less since t_0 is later than r/c and so closer to the TOGA (t_0 can be even later than the TOGA). The measured slope of the regression line fit, -0.008 cycles/kHz, means that the TOGA is 8 μ s after the sferic capture time, t_0 . Thus if we measure the phase, $\phi(\omega)$, at time $t_0 + 8 \mu$ s, the regression line is nearly horizontal as shown in Fig. 8(b).

If the sferic waveform is the sum of just two modes but one is dominant throughout the frequency range, the effect of the minor mode is a wavelike departure from a smooth curve as is possibly the case in Fig. 8. However, just as mode dominance can change with distance at a single frequency, mode dominance can change with frequency at a fixed distance, r . Fig. 9 shows such a case. At low frequencies (< 9 kHz), one mode is dominant. At high frequencies (> 10 kHz) a different mode (with different phase velocity) is dominant. This can be understood with the help of the phasor diagram (Fig. 10). This shows the mode A phasor as the thick arrowed line. The mode B phasor is represented by the thin arrowed line. Both rotate anticlockwise with frequency but the mode B phasor rotates faster (meaning $d\phi/d\omega$ is larger). The resultant is represented by the dashed arrowed line which rotates with frequency about the origin, O. With increasing frequency (indicated by numbers, 1, 2, 3, 4), mode A, initially dominant, becomes progressively weaker and mode B becomes progressively stronger. At the

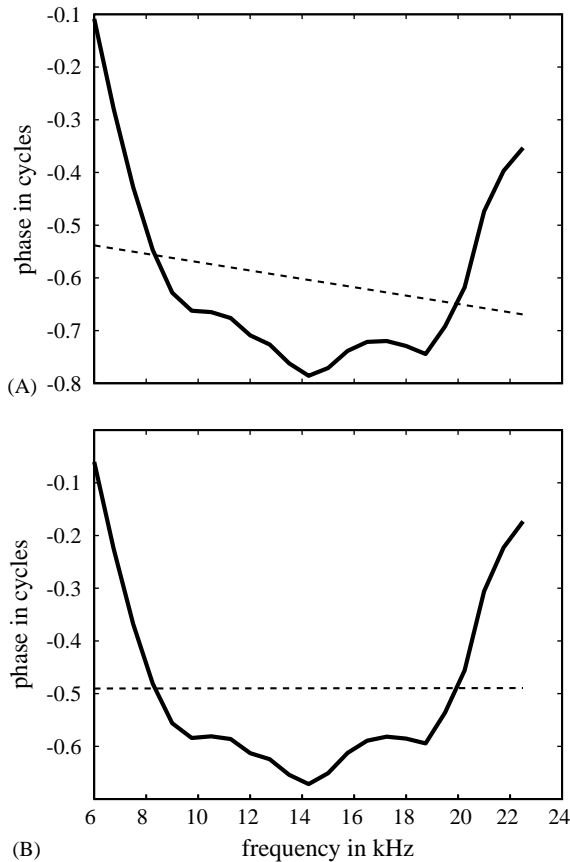


Fig. 8. Upper panel (a) shows the phase versus frequency (solid curve) at t_0 (trigger time) of a typical actual sferic. The slope of the regression line (-0.008 cycles/kHz) puts the TOGA at $t_0 + 8 \mu\text{s}$. Lower panel (b) shows the phase versus frequency at $t_0 + 8 \mu\text{s}$ to show that the slope of the regression line becomes zero at the TOGA.

frequency (between 9 and 10 kHz and represented in Fig. 10 by phasor sets 2 and 3) for which the two modes have equal amplitude, the phases in this case are nearly opposite. This produces a deep null in the amplitude spectrum (Fig. 11) and a half-cycle phase jump in the phase versus frequency (from -0.3 to -0.8 in Fig. 9). At higher frequencies, mode B is dominant.

This is an extreme case: the two modes at this frequency are just as likely to have the same phase (no phase jump) or have any other phase difference (less than a half-cycle jump). In any case, the slope of the regression line is affected in varying degrees by the phase jump.

Such phase jumps due to modal interference are not a problem in VLF lightning location. A given lightning stroke is likely to be received at many sites, even at those over 10 Mm distant. For example, suppose it is received at six sites, A, B, C, D, E, and F. Extreme interference (equal amplitude and opposite phase), if it occurs at all, is very unlikely to occur on more than one lightning-to-receiver

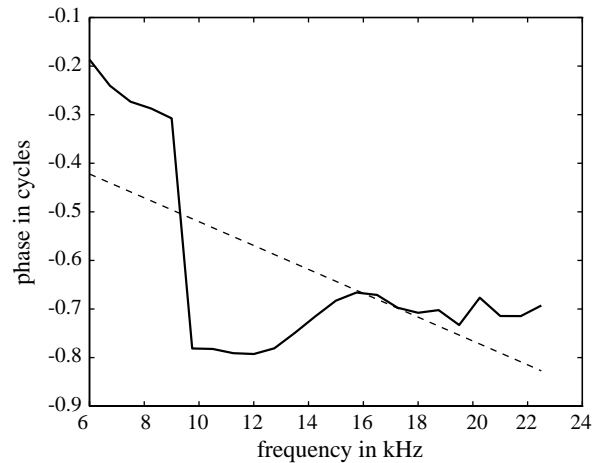


Fig. 9. Phase versus frequency at t_0 of a rare sferic exhibiting a phase jump of nearly 0.5 cycles ($\sim 180^\circ$). In consequence, the slope of the regression line is in error by $27 \mu\text{s}$ as deduced by hand removal of the phase jump. Only about 1% of phase jumps are as much as 180° which requires two modes almost equal in amplitude and opposite in phase. Such an error is easily detected and removed if five or more receiving sites detect the same lightning stroke.

path. Using the downhill simplex method on four of the six in turn (ABCD, BCDE, CDEF), the “bad” path is easily identified from the minimising residuals and so omitted from the location determination.

After examining the $\phi(\omega)$ plots of several hundred sferics it was decided that using the least-squares regression line gave the best estimate of phase slope in all cases for the time being. This is partly because the trigger time, t_0 , is often within $20 \mu\text{s}$ (one sample period) of the TOGA. The synthetic sferics in Figs. 3(b), 3(c) and 3(d) show that the TOGA occurs at or close to the maximum slope, $|dE/dt|$, which is where trigger capture is most likely for weak sferics. In fact, $|TOGA - t_0| > 100 \mu\text{s}$ is evidence of a bad measurement, allowing one to omit it for location if there are good measurements at four other sites. On the other hand, for strong sferics (as identified by the value of nJ/m^2 as discussed below in Section 4.1), $|dE/dt|$ can be adequate to trigger capture well before the maximum slope and so give large values of TOGA $-t_0$ not due to “bad” sferics.

4. TOGA potential and comparisons

4.1. TOGA measurement and errors

Fig. 12 shows the full waveform of the sferic considered in Fig. 8. As explained below in this section, only 64 samples are saved on sferic detection, the 16th (I_{ig}) being the sample which triggered the capture. As seen in Fig. 12 this set of 64 samples (1.3 ms) captures virtually all of the sferic except the long ringing at the waveguide cutoff frequency sometimes observed (as “tweaks”) in sferics which have

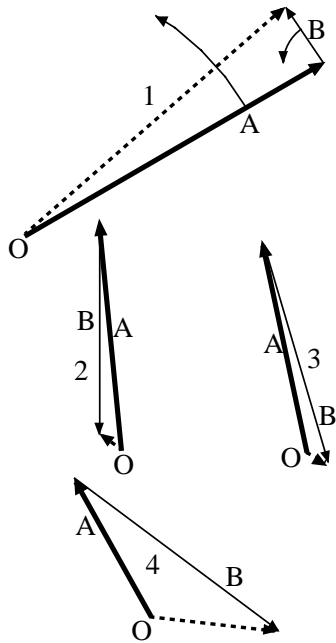


Fig. 10. This shows the mode A phasor, the mode B phasor and the resultant (dashed arrowed line) at progressively increasing frequency indicated by the numbers, 1, 2, 3, 4. Both A and B rotate ACW with frequency but the mode B phasor rotates faster (meaning $d\phi/d\omega$ is larger). Mode A, initially dominant, becomes progressively weaker and mode B becomes progressively stronger and eventually dominates. Phasor configurations 2 and 3 correspond to frequencies close to but on opposite sides of that for which the two modes have equal amplitude. Coincidentally, the phases of A and B in this case are nearly opposite, so the magnitude of the resultant is very small.

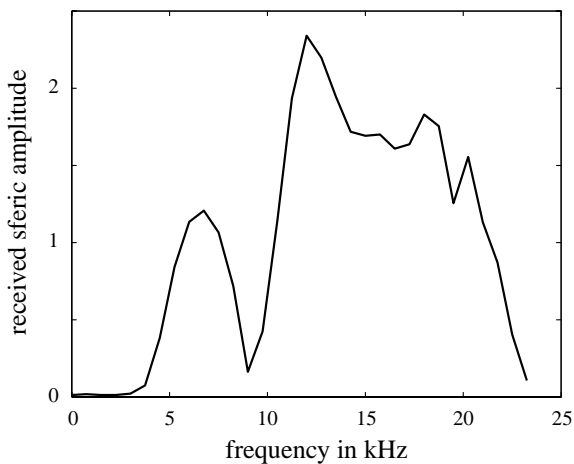


Fig. 11. Amplitude spectrum of the sferic showing the phase jump in Fig. 9. At the frequency of the phase jump this spectrum shows a deep minimum. This occurs because the two modes were almost equal in amplitude and opposite in phase at this frequency.

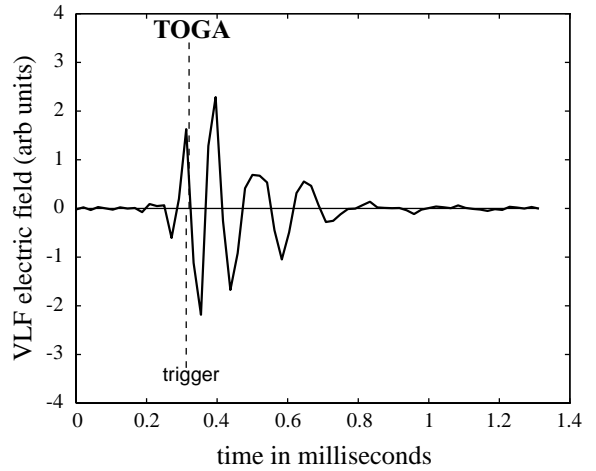


Fig. 12. This shows the full waveform of the sferic used for Fig. 8. Note that the sferic amplitude has dropped to the noise level by the end of the 1.3-ms duration of the 64 samples used (compared with 1024 used by Lee (1986a)). Using only 64 samples increases the signal (target sferic) to noise (VLF transmissions and other sferics) ratio and allows processible sferics to follow one another as closely as 2 ms. Also shown is the trigger point, t_0 , and the TOGA.

travelled long distances at night. Also shown is the trigger point t_0 , and the TOGA.

The ordinate in Fig. 12 is the VLF electric field in arbitrary units which are calibrated by the signal from the powerful (1 MW radiated) US Navy transmitter, NWC (19.8 kHz), 2000 km SW of Darwin. The unperturbed (by local site effects) electric field from NWC for near-noon propagation can be calculated (Morfitt and Shellman, 1976) and compared with the noon value in these arbitrary units. Integrating the squared values over the 64 samples of a captured sferic, with suitable scaling, gives the total VLF energy of the sferic passing through unit area at the receiver. For the sferic shown in Fig. 12, this is 50 nJ/m².

For the purpose of a rough estimate of the total VLF energy, ξ , radiated by a lightning discharge, we can assume that the energy propagates radially (horizontally) outward while restricted between the Earth's surface and the base of the ionosphere at altitude h . As the cylindrical wavefront of VLF energy expands radially, it loses some VLF energy into the ground and through the ionosphere. When the cylindrical wavefront has reached a radius (range) of r , the energy in the cylindrical wavefront, reduced to $\xi \exp(-\alpha r)$, is uniformly spread over a vertical cylinder of height h and radius r through which it is passing. Thus the energy flux density, W , in J/m² at range r is

$$W = \xi \exp(-\alpha r) / (2\pi r h) \tag{14}$$

so that

$$\xi = 2\pi r h W \exp(\alpha r), \tag{15}$$

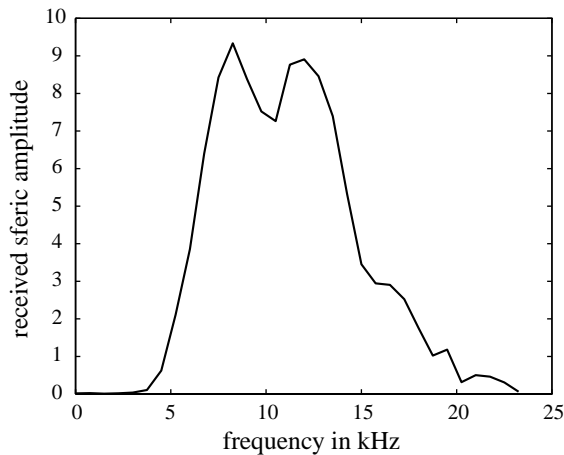


Fig. 13. Amplitude spectrum of the sferic of Figs. 8 and 12. Most of the energy is in the band 5–20 kHz. The two peaks at about 8 and 12 kHz, and weak minimum at about 10 kHz, show the presence of a higher order mode having an amplitude of about 12% of that of the dominant mode. This effect is also seen in Fig. 9.

where $h \sim 70$ km for daylight propagation and 90 km for nighttime propagation.

For example, we calculate ξ for the sferic shown in Fig. 12, for which $W = 50 \times 10^{-9} \text{ J/m}^2$. We will suppose $r = 1.5 \times 10^6 \text{ m}$, $h \sim 80$ km and suppose an attenuation of 2 dB/Mm. This makes the attenuation factor, $\exp(\alpha r)$ in Eq. (15), about 5. Substituting these in Eq. (15), we find $\xi \sim 200 \text{ kJ}$. Noting that the duration of the sferic shown in Fig. 12 is $< 1 \text{ ms}$, the average radiated power by the lightning discharge is $> 200 \text{ MW}$.

As explained above in Section 1.2, we determine lightning locations by the downhill simplex method of successive approximations. At some stage during this process, when the location residuals are < 30 km, say, we can use the group travel time and the attenuation appropriate for each path (Morfitt and Shellman, 1976) for all later iterations. Thus we can find the sferic energy flux density, W , at each site due to a “standard” lightning discharge of, say, 100 MJ, allowing ξ to be found from the W values by simple proportion.

Currently, NLDN determines and tabulates the peak current of the discharge (first return stroke) deduced from the peak electric field observed assuming an effective vertical length of the stroke path (Cummins et al., 1998). Elucidation of sprites and elves requires the charge moment or total charge transfer in a cloud-ground lightning discharge (Huang et al., 1999). Such can be more directly estimated from the total radiated energy, ξ , for estimated cloud-ground potentials or discharge lengths, than from the peak electric field of sferics measured at the NLDN sensors.

Fig. 13 shows the amplitude spectrum of the sferic in Fig. 12. By using only 64 samples (1.3 ms) the sferic dominates the background, so that the NWC signal at 19.8 kHz, which is the main contributor to the background, barely shows in

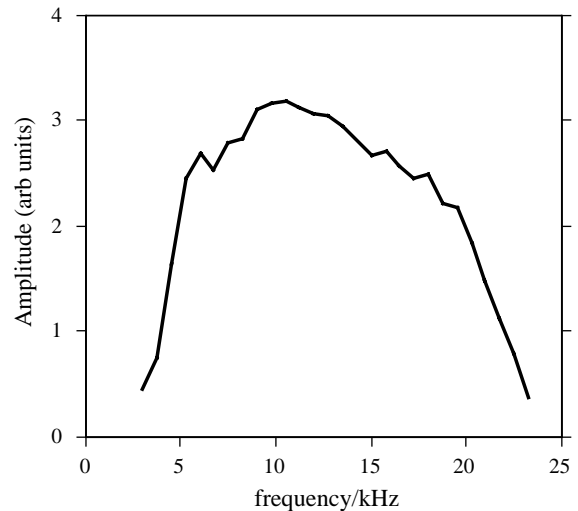


Fig. 14. Average amplitude spectrum obtained by taking the mean amplitude at each frequency (0–24 kHz in steps of 750 Hz) of 100 spectra of sferics recorded at Darwin, Australia. This has been corrected for the VLF receiver and sound card response as explained in the text. Maximum amplitude is at about 10 kHz, with half power points (3 dB) at about 5 and 19 kHz. This is in agreement with the lightning power spectrum from 1 kHz to 200 MHz shown by Malan (1963).

Fig. 13. Had we used 512 samples, as done for locating the GPS PPS, the NWC signal would have appeared nearly 20 dB stronger.

Fig. 14 shows the corrected amplitude spectrum of the average of 100 sferics. As in Fig. 13, the frequency scale (0–24 kHz) is spanned by 32 frequencies, 750 Hz apart, with no smoothing in frequency.

To ensure that this is the true spectrum of sferics, the amplitude response of the whole TOGA receiver, VLF antenna to computer, a white noise generator was fed into a dummy antenna (series 15 pF capacitor) for logging on the computer. Then from 750 DFTs, of 64 samples each, of this logged noise, the average spectrum, and so the TOGA system (including computer sound card) amplitude response, was found. The uncorrected amplitude spectrum of the average of 100 sferics (a vector of 32 terms) was divided term-by-term by the TOGA response (a vector of 32 terms) to produce the corrected spectrum shown in Fig. 14.

Maximum amplitude occurs at about 10 kHz. This is in agreement with the lightning power spectrum from 1 kHz to 200 MHz shown by Malan (1963). In terms of this vast range of nearly 18 octaves, the power spectrum of sferics is relatively narrow with the half power band (5–19 kHz from Fig. 14) covering < 2 octaves.

4.2. TOGA location measurement and errors

The random location error can be estimated from the residuals in the downhill simplex method of successive

approximations. Systematic errors can be detected by comparison with locations made by MF methods such as LPATS and IMPACT in geographical areas where these methods have highest accuracy.

In the early iterations of the downhill simplex method, while the approximate position of the lightning is unknown, we require an approximate group velocity which can be used for all paths at all times and frequencies about the spheric spectral peak. Watt (1967) shows the day and night group velocities for the first-order mode. At frequencies above 13 kHz, daytime velocities are higher than nighttime velocities while the reverse is true for frequencies below 12 kHz. Watt points out (p. 384) that “there is a frequency at which the group velocity during the day is equal to that at night somewhere in the 12–13 kc/s region”. At this “cross over” frequency, inspection of Watt’s Fig. 3.5.59 shows that $v_g = 0.9922c$, where c is the speed of light in vacuo, so that $v_g = 297.5$ m/ μ s across the Earth’s surface. It is interesting to compare these figures with those deduced for the synthetic spheric in Fig. 3 of 12.757 kHz and $v_g = 0.9914c$. As seen in Section 4.1 above (Fig. 14), the average spectral density of spherics is maximum near 10 kHz and only 5% below this maximum at 12.75 kHz.

Path propagation is also affected by ionospheric disturbances such as those produced by solar flares. However, the occurrence and estimated effect of solar flares are broadcast by space weather services. Thus, these can be incorporated into the propagation models used in the late iterations.

4.3. Comparison with the Omega navigation system

Until superseded by GPS, Omega provided a global positioning service utilising 8 VLF transmitters spaced around the world at precisely known locations. Each transmitter emitted four frequencies (10.2, 11.05, 11.333, and 13.6 kHz, being the multiples 36, 39, 40 and 48 of 283 1/3 Hz) in sequence. Users found their position from measurement of the received phases at each frequency from at least three of the Omega transmitters. These measurements provide 12 phase values, $\phi_i(\omega_j)$, corresponding to the three transmitters ($i = 1-3$) and the four frequencies ($j = 1-4$). All measurements were relative to the user’s standard which did not need to be absolute or even very stable since only differences were needed. The standard procedure was to use the differences, $\phi_1(\omega_j) - \phi_2(\omega_j)$ and $\phi_2(\omega_j) - \phi_3(\omega_j)$ at each frequency, ω_j . The third difference, $(\phi_1(\omega_j) - \phi_3(\omega_j))$, is simply the sum of the previous two differences. However, in principle, one could have used the same $\phi_i(\omega_j)$ data to find the derivatives, $(d\phi/d\omega)_i$, for each of the three Omega stations and so (via the time of group arrival or TOGA) the distance to each Omega station and consequently one’s position. Alternatively, if one knows one’s distance from an Omega station accurately, one could measure and use $d\phi/d\omega$ to get the absolute time accurately (Young and Thomson, 1994).

The TOGA method of lightning location is a kind of “inverse Omega” where the transmitter (lightning stroke) loca-

tion is unknown while the receivers are at precisely known locations. The VLF band utilised by TOGA includes that utilised by Omega, so the vast amount of research (thousands of publications, Swanson, 1981) on Omega, particularly on propagation, can be drawn on by TOGA. Even with only eight Omega transmitters around the world, all eight were detectable in many locations (Swanson, 1981) although only three were required for one’s position. We have already seen above (Fig. 1) that lightning as far away at 10 Mm can be located at VLF. It therefore seems likely that a global service of lightning location could be provided with only about 10 well-placed TOGA stations.

The phase and group velocity vary with frequency, ionospheric conductivity and height, ground conductivity, etc. (Morris and Milton, 1974). To convert phase differences and so time to range and position, the Omega system used a nominal value of phase velocity of $c/0.9974$ which is an average of the dominant phase velocity over all paths and time (Jones and Mowforth, 1981). This is a rather gross approximation considering the large change in phase velocity ($\sim 0.4\%$) from night to day at Omega frequencies (Watt, 1967) compared with our use of a group velocity of $0.9922c$ which is the same for both day and night paths as discussed in Section 4.1. Under normal conditions, the locations by Omega were accurate to within about 3 km. Errors could be reduced to 1–2 km by applying propagation corrections (Swanson, 1981). Under unusual conditions ($\sim 0.2\%$ of the time) due to solar flares, errors could be > 8 km. Thus, by comparison with Omega, we would expect at least the same accuracy for TOGA location of lightning.

As is seen from the citation dates above, the technology available to Omega was that of over 20 years ago. In particular, computer power has increased by over two orders of magnitude in that time, so that sophisticated computer models of VLF propagation (Morfit and Shellman, 1976), incorporating ground conductivity maps and ionospheric models calculated for geographic, diurnal, seasonal and solar conditions, can be used to calculate the modal structure and group velocities of propagation for use in the later iterations of the downhill simplex method of successive approximations.

4.4. Comparison with ATD by cross-correlation

Since location requires only the ATDs, in the system described by Lee (1986a, 1986b, 1989), the ATD is found directly by cross-correlating the two VLF wave trains (spherics) from each independent pair of receiver sites. To distinguish his method from TOA methods such as LPATS (Casper and Bent, 1992), Lee (1986a) refers to his method as “ATD”. Since both Lee’s ATD and our TOGA use the VLF band (though Lee’s lightning reception extends into the LF), the advantages of VLF use, particularly the very long range, apply to both as do the errors due to propagation experienced by Omega.

However, the advantage of using the TOGA method is that the ATD for any pair of receiver stations is simply the

difference between two numbers (the two TOGAs) while cross-correlation requires comparison of two wave trains, which in Lee's form (Lee, 1986a, 1989) consist of 1024 samples. Typically, each TOGA station detects and transmits the TOGA (and other parameters) of 100,000 sferics per day to a central point for lightning stroke location analysis. This requires about 1 Mbyte/day/station. 100,000 sferic waveforms of 1024 samples, as well as the detection time (t_0), per day would seem to require over 100 Mbyte/day/station.

4.5. VLF versus MF lightning location

The advantages of VLF methods of lightning location are the long ranges allowed by the low attenuation of VLF propagation in the Earth–ionosphere waveguide. This in turn allows a low density of receiver stations which can be about 10–30 times further apart (100–1000 times lower density) than the density (10 Mm^{-2}) required by the TOA methods described earlier. In fact, such a low density, and so low cost of service per square megametre, is the only economically feasible way to provide a real time service to vast areas of unpopulated ground or ocean, or vast areas populated by people unable to afford the costs required of a high site density network like NLDN. Despite the vast decrease in site (receiver station) density, current VLF lightning location (Lee, 1989) and Omega (Swanson, 1981) indicate an obtainable location accuracy of 1–2 km compared with the median accuracy of NLDN of 0.5 km, only a three-fold decrease.

Lightning is an indicator or proxy for severe weather (Markson and Ruhnke, 1999). Lightning location and tracking made available in real time would be of particular use for “now casting” in remote areas to give advanced warning of severe weather hazards to airliners or ships, or via civil defence and similar bodies, to aircraft and boats. Since VLF sferics are produced almost exclusively by cloud-ground return strokes (Pierce, 1977) and are radiated from within 2 km of the ground (see Section 2.1 above), VLF location finds the ground striking point like LPATS does but with lower accuracy. Thus VLF location may meet the needs of foresters, farmers, even power transmission line operators. Where the average lightning location in a moving thundercloud is of prime interest, it is worth noting that the location error of VLF methods for individual lightning strokes (1–2 km) is much less than the spread of ground strike positions (up to 10 km) of strokes in a single flash (Cummins et al., 1998).

5. Conclusions

At VLF, the relatively slow onset of lightning sferics precludes accurate measurement of the “time of arrival” (TOA) as used by LPATS in dense networks like the US NLDN in several countries around the world. However, the “time of group arrival” (TOGA), determined from the phase slope

with respect to frequency over the range 6–22 kHz, can be found to within 1 μs in good conditions. By analogy with the (now defunct) Omega Navigation System, which used discrete frequencies in the range 10–14 kHz, lightning location errors using TOGA should be only 1–2 km. While this is about three times the errors of location by LPATS, the areal density (lightning sensors per square megametre) required by a TOGA network is some 100–1000 times less than that required by an LPATS network so that, like Omega, a truly global service can be provided by only about 10 TOGA sites.

Acknowledgements

We thank the University of Otago, Dunedin, New Zealand; Northern Territory University, Darwin, Australia; Murdoch University, Perth, Australia; Griffith University, Brisbane, Australia; Osaka University, Japan; and the National University of Singapore, Singapore, for housing our VLF lightning acquisition receivers. We are indebted to Dr. Neil Thomson of the University of Otago, Dunedin, New Zealand, for many helpful discussions and suggestions in this research.

References

- Casper, P.W., Bent, R.B., 1992. Results from the LPATS USA national lightning and tracking system for the 1991 lightning season. Proceedings of the 21st International Conference Lightning Protection, Berlin, Germany, September, pp. 339–342.
- Cheng, D.K., 1983. *Field and Wave Electromagnetics*. Addison-Wesley, Reading, MA.
- Cummins, K.L., Murphy, M.J., 2000. Overview of lightning detection in the VLF, LF, and VHF frequency ranges. Presented at 2000 International Lightning Detection Conference, Tucson, Arizona, 7–8 November, pp. 1–10.
- Cummins, K.L., Krider, E.P., Malone, M.D., 1998. The US national lightning detection network and applications of cloud-to-ground lightning data by electric power utilities. *IEEE Transactions on Electromagnetic Compatibility* 40 (4), 465–480.
- Huang, E., Williams, E., Boldi, R., Heckman, S., Lyons, W., Taylor, M., Nelson, T., Wong, C., 1999. Criteria for sprites and elves based on Schumann resonance observations. *Journal of Geophysical Research* 104 (D14), 16,943–16,964.
- Jones, T.E., Mowforth, K., 1981. The effects of propagation on the accuracy of positions determined using Omega in the U K. Presented at the AGARD Symposium on Medium, Long and Very Long Wave Propagation, Conference Proceedings, Brussels, Belgium, pp. 37:1–37:30.
- Krider, E.P., Noggle, R.C., Uman, M.A., 1976. A gated wideband magnetic direction finder for lightning return strokes. *Journal of Applied Meteorology* 15, 301–306.
- Lee, A.C.L., 1986a. An experimental study of the remote location of lightning flashes using a VLF arrival time difference technique. *Quarterly Journal of the Royal Meteorological Society* 112, 203–229.

- Lee, A.C.L., 1986b. An operational system for the remote location of lightning flashes using a VLF arrival time difference technique. *Journal of Atmospheric and Oceanic Technology* 3, 630–642.
- Lee, A.C.L., 1989. Ground truth confirmation and theoretical limits of an experimental VLF arrival time difference lightning flash locating system. *Quarterly Journal of the Royal Meteorological Society* 115, 1147–1166.
- Lewis, E.A., Harvey, R.B., Rasmussen, J.E., 1960. Hyperbolic direction finding with sferics of transatlantic origin. *Journal of Geophysical Research* 65, 1879–1905.
- Malan, D.J., 1963. *Physics of Lightning*. The English Universities Press, London.
- Markson, R. J., Ruhnke, L. H., 1999. New technology for mapping total lightning with groundbased and airborne sensors. Abstract E1.2, URSI Abstracts 265.
- Morfitt, D. G., Shellman, C. H., 1976. MODESRCH: an improved computer program for obtaining ELF/VLF/LF propagation data. Technical Report NOSC/TR 141, Nav. Ocean Syst. Cent., San Diego, CA.
- Morris, P. B., Milton, Y. C., 1974. Omega propagation corrections: background and computational algorithm. ONSOD Report No. ONSOD-01-74.
- Pierce, E.T., 1977. Atmospherics and radio noise. In: Golde, R.H. (Ed.), *Lightning 1: Physics of Lightning*, pp. 351–384.
- Swanson, E.R., 1981. Omega. Presented at the AGARD Symposium on Medium, Long and Very Long Wave Propagation, Conference Proceedings, Brussels, Belgium, pp. 36:1–36:16.
- Trimble Navigation Ltd., 1999. *Lassen SK II GPS. System Designer Reference Manual*, Sunnyvale, USA.
- Uman, M.A., 1983. *Lightning*. Dover, New York.
- Watt, A.D., 1967. VLF radio engineering. *International Monographs in Electromagnetic Waves*, Vol. 14. Pergamon, Oxford, England.
- Young, W.F., Thomson, N.R., 1994. Time of day from Omega VLF signals. *Measurement Science and Technology* 5, 1202–1209.